



Numerical Simulation and Deep Neural Network Revealed Drag Reduction of Microstructured Three-Dimensional Square Cylinders at High Reynolds Numbers

Siying Wang¹, Qibiao Wu¹ and Xiaotao Shi^{2*}

¹Department of Engineering Structure and Mechanics, School of Science, Wuhan University of Technology, Wuhan, China, ²Hubei International Science and Technology Cooperation Base of Fish Passage, China Three Gorges University, Yichang, China

OPEN ACCESS

Edited by:

Gongfa Li,
Wuhan University of Science and
Technology, China

Reviewed by:

Yongqiang Sha,
Huaqiao University, China
Guoming Zeng,
Chongqing University of Science and
Technology, China
Lahouari Adjilout,
Oran University of Science and
Technology–Mohamed Boudiaf,
Algeria

*Correspondence:

Xiaotao Shi
sxtshanghai@163.com

Specialty section:

This article was submitted to
Bionics and Biomimetics,
a section of the journal
Frontiers in Bioengineering and
Biotechnology

Received: 28 February 2022

Accepted: 13 May 2022

Published: 29 June 2022

Citation:

Wang S, Wu Q and Shi X (2022)
Numerical Simulation and Deep Neural
Network Revealed Drag Reduction of
Microstructured Three-Dimensional
Square Cylinders at High
Reynolds Numbers.
Front. Bioeng. Biotechnol. 10:885962.
doi: 10.3389/fbioe.2022.885962

Square cylinders are widely used in various fields. For example, they are common structures in fishways. The flow around square cylinders has been a common problem in various fields. However, reducing the flow drag of the square cylinder is a problem that remains unexplored. Many previous studies have reported the drag reduction of 2D square cylinders, which failed to reflect the drag of real structures. Also, some studies focus on the drag force of the inner wall of the square cylinder modified by the microstructure. Achieving drag reduction by microstructuring the surface of the 3D square cylinder is a challenging problem. This study applied a 3D numerical simulation and deep neural network to study the drag reduction performance of the square cylinder under different patch sizes. We studied the drag reduction performance of protrusion and pit-patched square cylinders and tried to find the rule between drag reduction performance and patch configuration. The results show that the square cylinder has better drag reduction performance in some cases. However, its drag reduction performance is greatly affected by the protrusion structure. Also, too large protrusions will increase the drag force of the structure. When the surface protrusion accounts for 10% of the total area of the square cylinder, the drag reduction performance is the best (22.1%). The pit patch structure demonstrated an insignificant drag reduction performance and even increased the drag in most cases. The DNN prediction model demonstrated the robustness of the numerical simulation data.

Keywords: square cylinder, numerical simulation, passive control, drag reduction, neural network

INTRODUCTION

Square cylinders are widely used in the engineering field, and they are common structures in fishways. A square cylinder can be regarded as a bluff body structure with a rectangular cross section, such as cylinders, beams, and fences in the building structure (Chen, 2019; Shui et al., 2021; Yang et al., 2021). In fluid mechanics, the flow around a square cylinder is a classic problem of flow around a bluff body, which contains complex phenomena such as impact, separation, reattachment, orbiting, and vortex often encountered in various fields (Lahaye et al., 2014; Vikram et al., 2020). In

TABLE 1 | Various parameters were used to model the flow past the square cylinder.

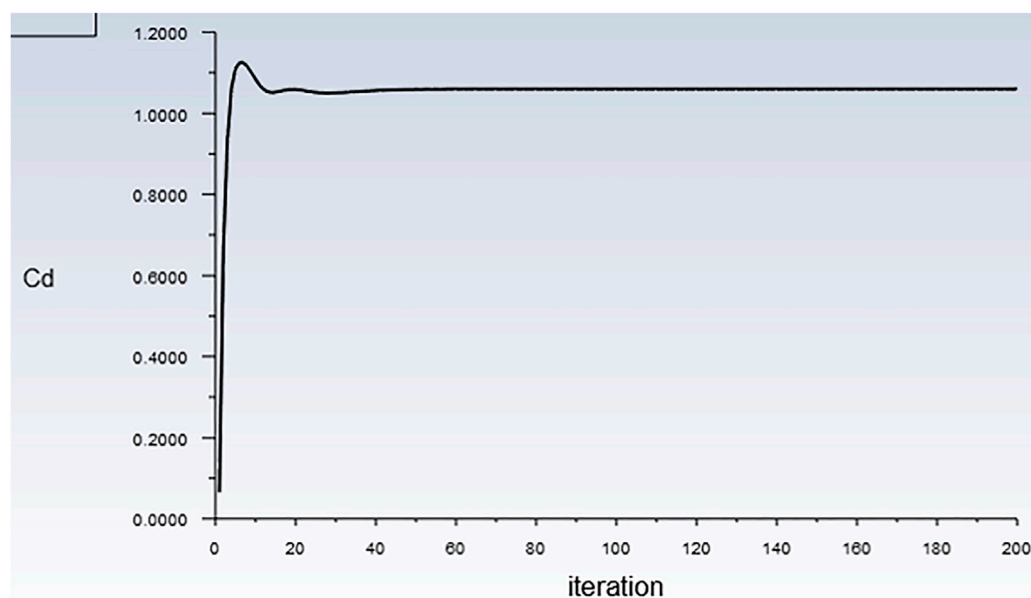
Surface pit ratio	b/20	1%	5%	10%	20%	30%	50%
Value	b(mm)	0.2	1	2	4	6	10

addition, many engineering structures and marine cylinder structures involve flow around square cylinders (Behera and Saha, 2021). The study on square cylinders generally focuses on the drag and lift forces and the local instability oscillation caused by the periodic change of both forces.

Researchers have conducted wind tunnel experiments on the flow around the square cylinder (Wang et al., 2021; Zhao et al., 2021). However, the wind tunnel experiment is costly and inefficient in obtaining large experimental data. Compared with traditional experiments, numerical simulation and algorithms have the advantages of convenient modeling, low cost, and high computational efficiency for predicting mechanical behavior (Sun et al., 2020a; Luo et al., 2020; Ma et al., 2020). It can also conveniently simulate complex structures' flow fields and assist engineering problems effectively. Numerical simulation has been widely used in the drag reduction study of various bluff bodies, including square cylinders (Bearman, 1998). Researchers have shown great interest in the flow around square cylinders (Yen and Wu, 2012). The drag reduction control methods for bluff body flow are mainly divided into active and passive control methods. The active control aims to regulate the flow by applying additional external energy. The passive control method changed the shape of the bluff body or added other microstructures. The passive control method is simpler and less expensive (Koide et al., 2006; Kim and Kim, 2012; Bahrami and Hacısevki, 2019).

When the fluid flows through the front edge of the square cylinder, the surface of the square cylinder will hinder the fluid. Also, the high-pressure fluid near the front edge promotes the developing boundary layer to gradually develop to both sides of the square cylinder. Blockage occurs under the influence of viscosity, which loses kinetic energy and causes the fluid to slow down gradually. At the same time, the force generated by the pressure is not enough to surround the entire back of the square cylinder under the high Reynolds number. Still, a separation point is generated near the maximum width of the square cylinder, and the separated fluid forms an unstable shear layer. Since the flow velocity of the outer part near the free flow area is greater than that of the inner part, the fluid tends to rotate and disperse into several vortices. In addition, the strength of the vortex gradually weakens due to the existence of fluid viscosity during the downstream movement of the vortex. After the boundary layer detaches from the surface at the separation point, a wake area is formed at the tail of the square cylinder. Also, the surrounding flow drag is formed under the action of the pressure difference between the front edge and the wake area. When the separation point is further back, the wake area is smaller. Also, the pressure difference resistance acting on the square cylinder is smaller to reduce the drag.

Authors previously reduced drag force by placing cylinders upstream of square cylinders. Earlier, Lesage and Gartshore (1987) placed two-dimensional (2D) plates, circular cylinders, and square cylinders upstream and computed their drag force. Their work has shown that the drag force of superimposed bluff bodies with other cylinders is significantly lower than that of a single bluff body. Igarashi (1997) and Mangal et al. (2014) also use small rods to reduce the drag force of the square cylinder. The authors also modified cylinder surfaces to reduce the drag force to simplify practical applications. He et al.

**FIGURE 1** | The iterative curve of the drag coefficient.

Forces - Direction Vector (1 0 0)						
Zone	Forces (n)			Coefficients		
	Pressure	Viscous	Total	Pressure	Viscous	Total
back	0.2186309	0	0.2186309	0.27106401	0	0.27106401
down	0	-0.0011139895	-0.0011139895	0	-0.0013811519	-0.0013811519
front	0.63962829	0	0.63962829	0.79302704	0	0.79302704
left	0	-0.001118046	-0.001118046	0	-0.0013861812	-0.0013861812
right	0	-0.0011063877	-0.0011063877	0	-0.001371727	-0.001371727
top	0	-0.0011065047	-0.0011065047	0	-0.001371872	-0.001371872
-----	-----	-----	-----	-----	-----	-----
Net	0.85825919	-0.0044449279	0.85381426	1.0640911	-0.005510932	1.0585801

FIGURE 2 | Drag force on all sides.

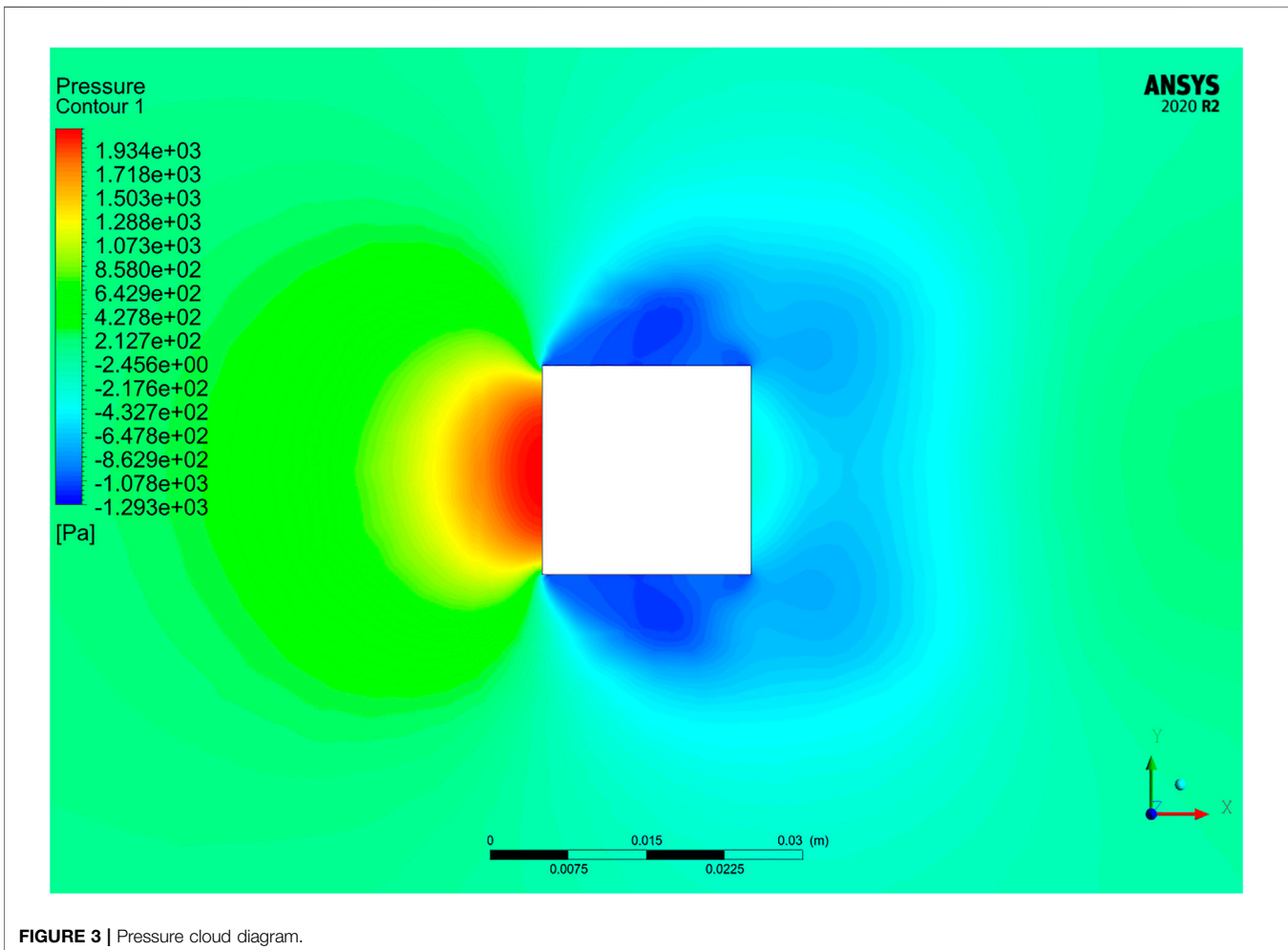


FIGURE 3 | Pressure cloud diagram.

(2014) used particle image velocimetry to study the flow around a square cylinder with front cut corners. The authors found that this structure reduced drag and discussed the fluid dynamical mechanism. Tong et al. (2015) used chamfered corners to reduce the drag of 2D square cylinders with a sharp-angled square and octagonal cross section. The authors found that the chamfered structure reduces drag force compared with sharp corners.

The study also reported microstructures to enhance cylindrical drag reduction. But these solutions are mostly used on the inner

wall of the pipes. Costantini et al. (2018) studied the drag reduction caused by the superhydrophobic surface with grooved microstructures in turbulent pipes. Jin et al. (2019) conducted a super large eddy simulation (VLES) on the passive drag reduction of a 2D square cylinder based on OpenFOAM. Lorite-Diez et al. (2020) studied the drag reduction of three-dimensional bluff bodies with different rear cavities under crosswind conditions. When the free flow is aligned with the object, the curved cavity provides stronger wave attenuation and wake bistableness than the straight

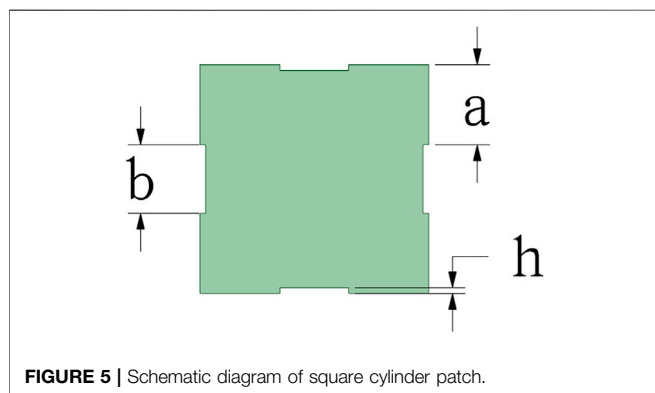
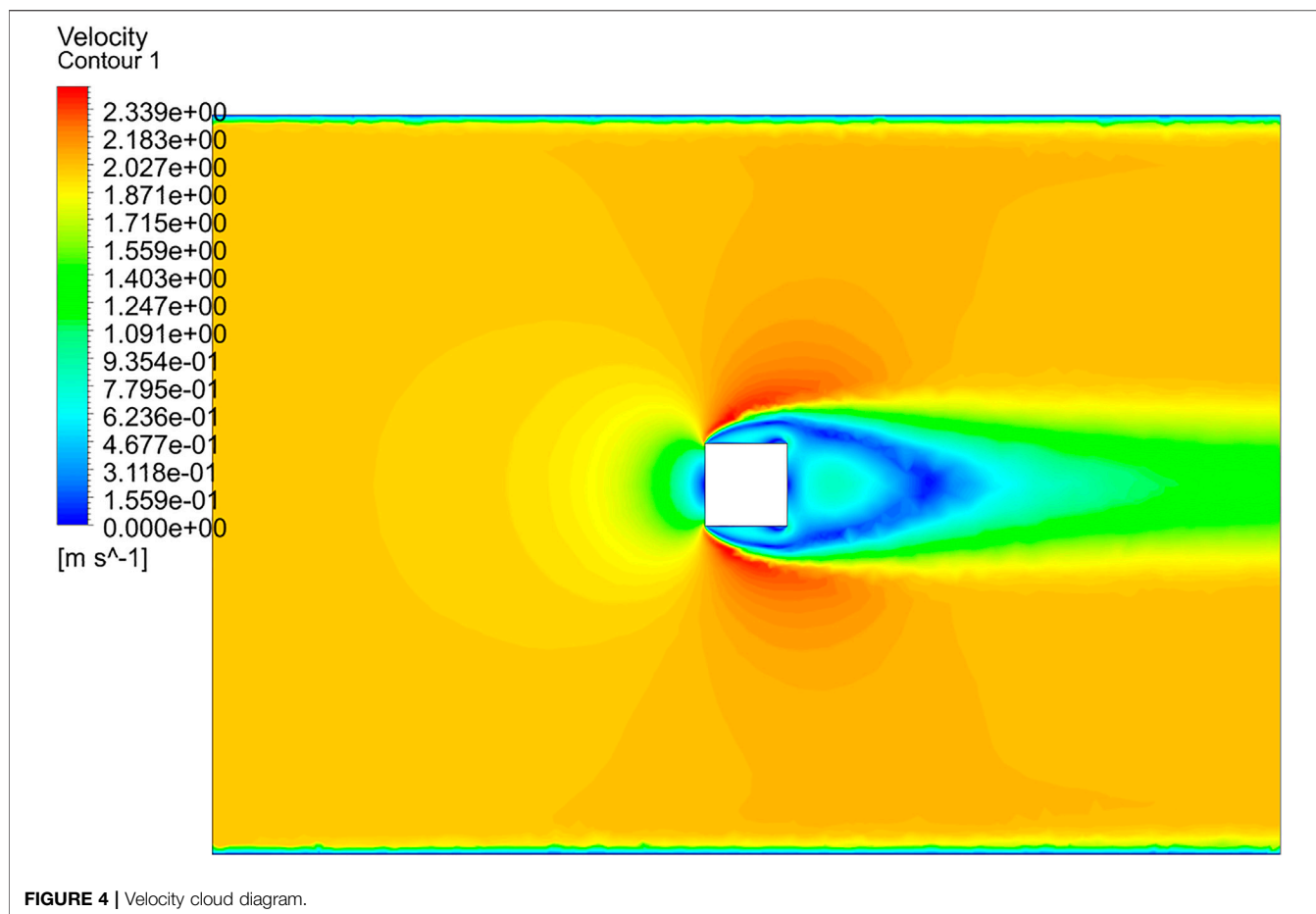


TABLE 2 | Different working conditions.

b (mm)	n	a (mm)	h (mm)
10	1	5	±0.5, ±1, ±2, ±3, ±4
6	1	7	±0.5, ±1, ±2, ±3, ±4, ±5, ±6
	2	3, 2, 3	±0.5, ±1, ±2
	3	0.5	±0.1, ±0.2, ±0.3, ±0.4
4	1	8	±0.5, ±1, ±2, ±3, ±4, ±5, ±6, ±7
	2	4	±0.5, ±1, ±2, ±3
	3	2	±0.5, ±1
2	1	9	±0.5, ±1, ±2, ±3, ±4, ±5, ±6, ±7, ±8
	2	6, 4, 6	±0.5, ±1, ±2, ±3, ±4, ±5
	3	3.5	±0.5, ±1, ±2, ±3
	4	2.4	±0.5, ±1, ±2
1	1	9.5	±0.5, ±1, ±2, ±3, ±4, ±5, ±6, ±7, ±8, ±9
	2	6	±0.5, ±1, ±2, ±3, ±4, ±5
	3	5, 3.5, 3.5, 5	±0.5, ±1, ±2, ±3, ±4
	4	3.2	±0.5, ±1, ±2, ±3
	5	2.5	±0.5, ±1, ±2
	6	2	±0.5, ±1

cavity. Moreover, the drag force of a curved cavity is smaller than that of a straight cavity. Machine learning and deep learning techniques have been widely used in engineering research (Jiang et al., 2021a; Jiang et al., 2021b; Huang et al., 2021; Huang et al., 2022). The neural network is a kind of neural network that simulates the human brain to realize artificial intelligence-like machine learning technology. This study also adopts a deep neural network for resistance prediction (DNN).

Many previous studies have reported the drag reduction of 2D square cylinders, which failed to reflect the drag of real structures.

Also, some studies focus on the drag force of the inner wall of the square cylinder modified by the microstructure. Reducing drag force by microstructured the outer surface of the square cylinder

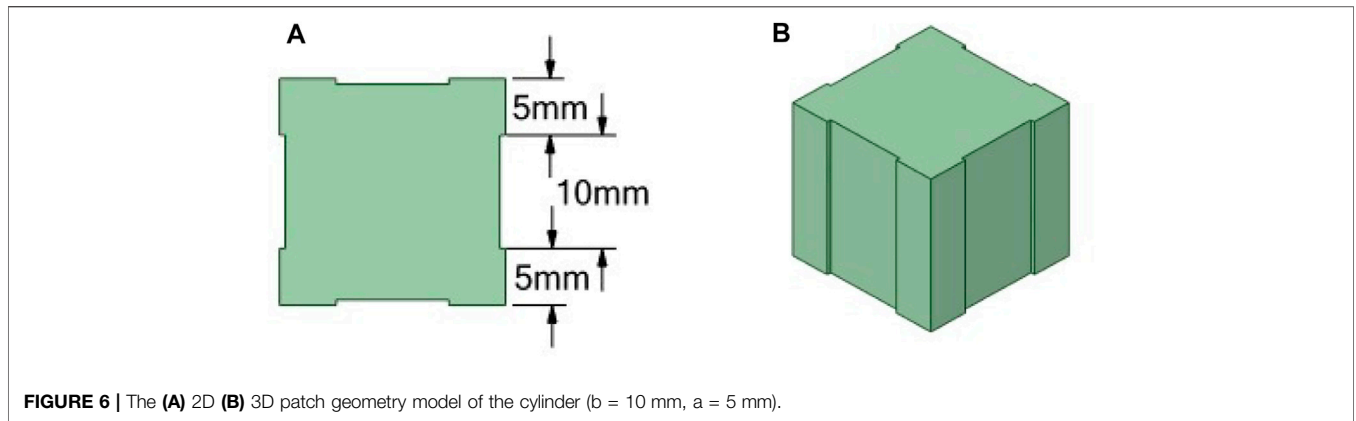


FIGURE 6 | The (A) 2D (B) 3D patch geometry model of the cylinder (b = 10 mm, a = 5 mm).

TABLE 3 | Values of the surface patch ratio.

Surface patch ratio	b/20	1%	5%	10%	20%	30%	50%
Value	b (mm)	0.2	1	2	4	6	10

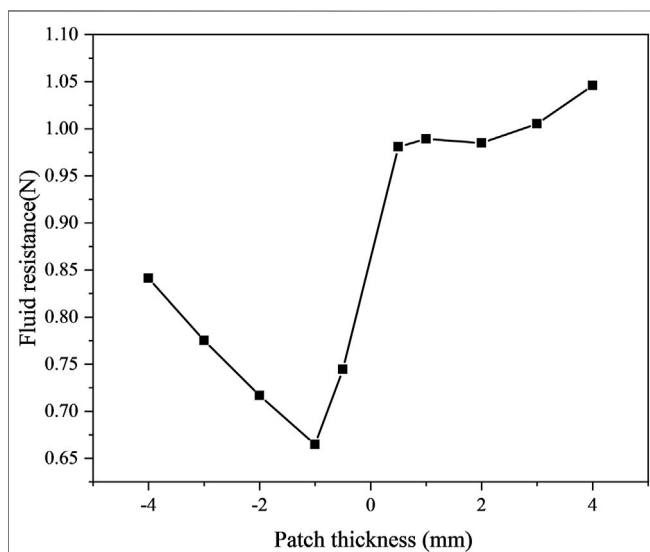


FIGURE 7 | The drag force under different patch thicknesses when b = 10 mm and a = 5 mm.

is a challenging problem. The study performed the 3D numerical simulation of the flow around the square cylinder based on the numerical simulation. The passive control method is used to achieve drag reduction by adding microstructured patches to the square cylinder. The square cylinder can be divided into convex and concave structures for simulation, including several patch sizes. The optimal drag reduction structure is finally found compared with the smooth square cylinder. Optimizing the surface structure can reduce drag and improve the stability of the structure of the square cylinder. For example, it may provide a reference for the supporting structure of the bridge underwater.

MATERIALS AND METHODS

Calculation Model

The Spalart-Allmaras turbulence model only needs to solve the transport equation. In the Spalart-Allmaras model, the transport variables are the same as the turbulent kinematic viscosity except for the near-wall (viscous effect) region. The transport equation for the modified turbulent viscosity is

$$\frac{\partial}{\partial t} (\rho \tilde{v}) + \frac{\partial}{\partial x_i} (\rho \tilde{v} u_i) = G_v + \frac{1}{\sigma_{\tilde{v}}} \left[\frac{\partial}{\partial x_j} \left\{ (\mu + \rho \tilde{v}) \frac{\partial \tilde{v}}{\partial x_j} \right\} + C_{b2} \rho \left(\frac{\partial \tilde{v}}{\partial x_j} \right)^2 \right] - Y_v + S_{\tilde{v}},$$

where G_v is the generation of turbulent viscosity, Y_v is the reduction in turbulent viscosity in the near-wall region. $\sigma_{\tilde{v}}$ and C_{b2} is a constant, ν is the molecular kinematic viscosity. $S_{\tilde{v}}$ is a user-defined source item.

At the wall, the turbulent kinematic viscosity is set to zero. When the calculation grid is fine enough to calculate the laminar bottom layer, the wall shear stress is solved by the laminar flow stress-strain relationship, namely,

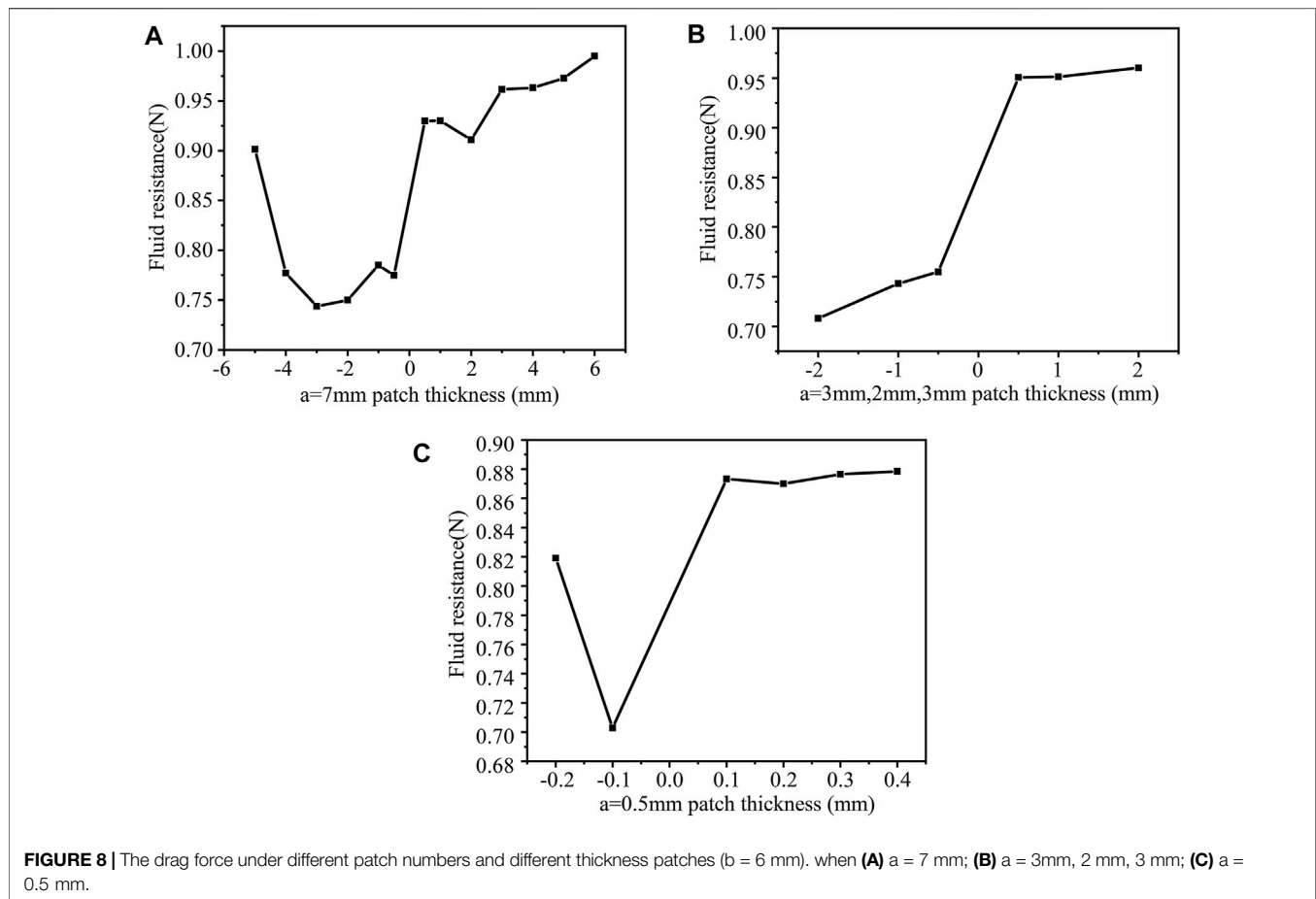
$$\frac{u}{u_\tau} = \frac{\rho u_\tau y}{\mu}.$$

Assuming that the centroid of the mesh adjacent to the wall falls in the logarithmic region of the boundary layer, then according to the wall law,

$$\frac{u}{u_\tau} = \frac{1}{k} \ln E \left(\frac{\rho u_\tau y}{\mu} \right), k = 0.4187, E = 9.793,$$

where u is the velocity parallel to the wall, u_τ is the friction velocity, and y is the distance from the wall.

- (1) The calculation area is 260 mm × 180 mm × 180 mm, the size of the square cylinder is 20 mm × 20 mm × 20 mm, and the square cylinder is located at the center of the calculation area. The distance between the square cylinder model and the velocity inlet and pressure outlet is 120 mm, and the model is 80 mm away from other boundaries.



- The fluid parameters are water, density 998.2 kg/m³, viscosity 0.001003 Pa.s, the left side is the water inlet velocity, the inlet velocity is 2 m/s, and the right side is the pressure outlet, the pressure is 0, around. It is a non-slip wall boundary condition.
- $Re \approx 40,000$ from the calculation parameters, and the Spalart-Allmaras turbulence model is selected to calculate the flow field. In this case, the model is valid for the wall in the near-wall area. Therefore, the requirements for the quality of the boundary layer grid are relatively high. There is no apparent interface between the fluid inside and outside the boundary layer. In practical applications, it is generally artificially stipulated that the boundary layer thickness is 0.99 times the free velocity from the wall to the flow velocity.

Calculation method of the thickness of the boundary layer of the flat plate:

$$\delta(L) = 0.035 \frac{L}{Re^{1/7}} \sim 0.214 \text{ mm.}$$

According to the thickness of the boundary layer calculated by the above formula, set the boundary layer as follows: Set the boundary layer around the square cylinder, the total thickness of the boundary layer is 10 mm, and there

are 20 layers in total, which meet the requirements of the above formula.

Grid setting: the grid size of the square cylinder surface is 0.5 mm, the grid size of other water areas except the boundary layer is 3 mm, and the total number of grids is 1.18 million. Various parameters are shown in **Table 1**.

Validation of the Numerical Simulation

Numerical results from other experiments are compared to validate the mathematical model. The calculated drag coefficient iteration curve is shown in **Figure 1**. According to the theory of fluid mechanics, the drag forces of an object completely immersed in the fluid are mainly composed of the pressure on the front and rear surfaces of the object and the viscous drag on the side. The pressure drag forces are decisive at higher Reynolds numbers. It can be seen from **Figure 2** that the drag force mainly includes the drag force of the pressure difference between the front and rear surfaces, which is consistent with the fluid mechanics' theory of the flow around the body. **Figure 3** shows that the pressure on the front surface is the largest, so the pressure drag forces were mainly provided by the front surface (0.6396N). **Figure 4** also shows that the velocity gradient on the left and right surfaces changes significantly, and the viscous force mainly comes from this. Thus, both sides mainly provide viscous drag forces. The numerical simulation results show that the pressure on the front and rear surfaces of the object primarily contributes to

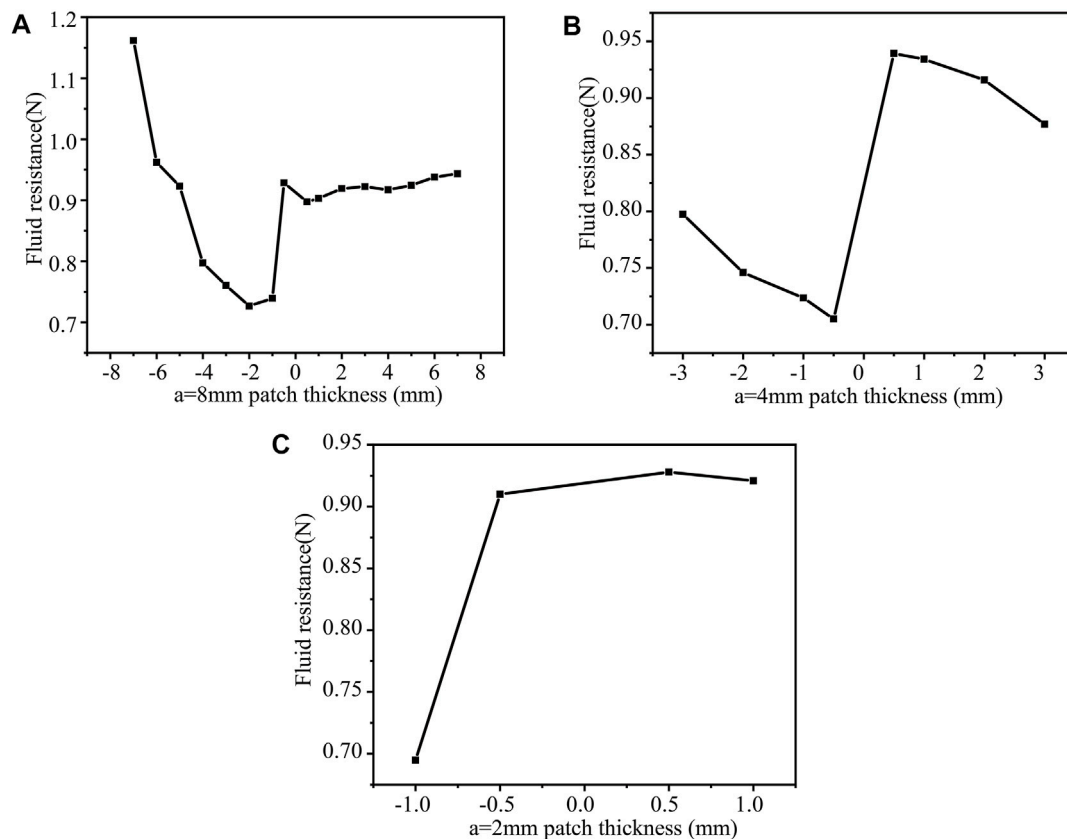


FIGURE 9 | $b = 4$ mm, the drag force under different patch numbers and different thickness patches (A) $a = 8$ mm; (B) $a = 4$ mm; (C) $a = 2$ mm.

the drag forces, which also validates that the pressure difference primarily contributes to the drag forces at high Reynolds numbers. Finally, the smooth square cylinder has a drag force of 0.85381 and a drag coefficient of 1.0585. The drag coefficient of the square cylinder obtained from the experiment is 1.05. The drag coefficient obtained by numerical simulation is close to the experiment and the relative error is 6.65%. It shows that the numerical simulation in this study is accurate and reliable.

Numerical Simulation Conditions

We tried to study the influence of different patch sizes on the drag force of the square cylinder. The patch size is shown in Figure 5, and the following equation needs to be satisfied:

$$\sum_{i=1}^{n+1} a_i + b * n = 20,$$

where n is the number of patches, b is the patch length, h is the patch width, and a is the interval length between patches. To ensure the integrity of the square cylinder, $h < a$ must be satisfied. When h takes a positive value, the patch is “sag.” Also, when h takes a negative value, the patch is “raised.” According to the requirements of the above geometric dimensions, the calculation can be divided into the following working conditions (Table 2). The result is measured by the ratio of the surface area occupied by the pits. For its drag reduction effect, some values of the surface

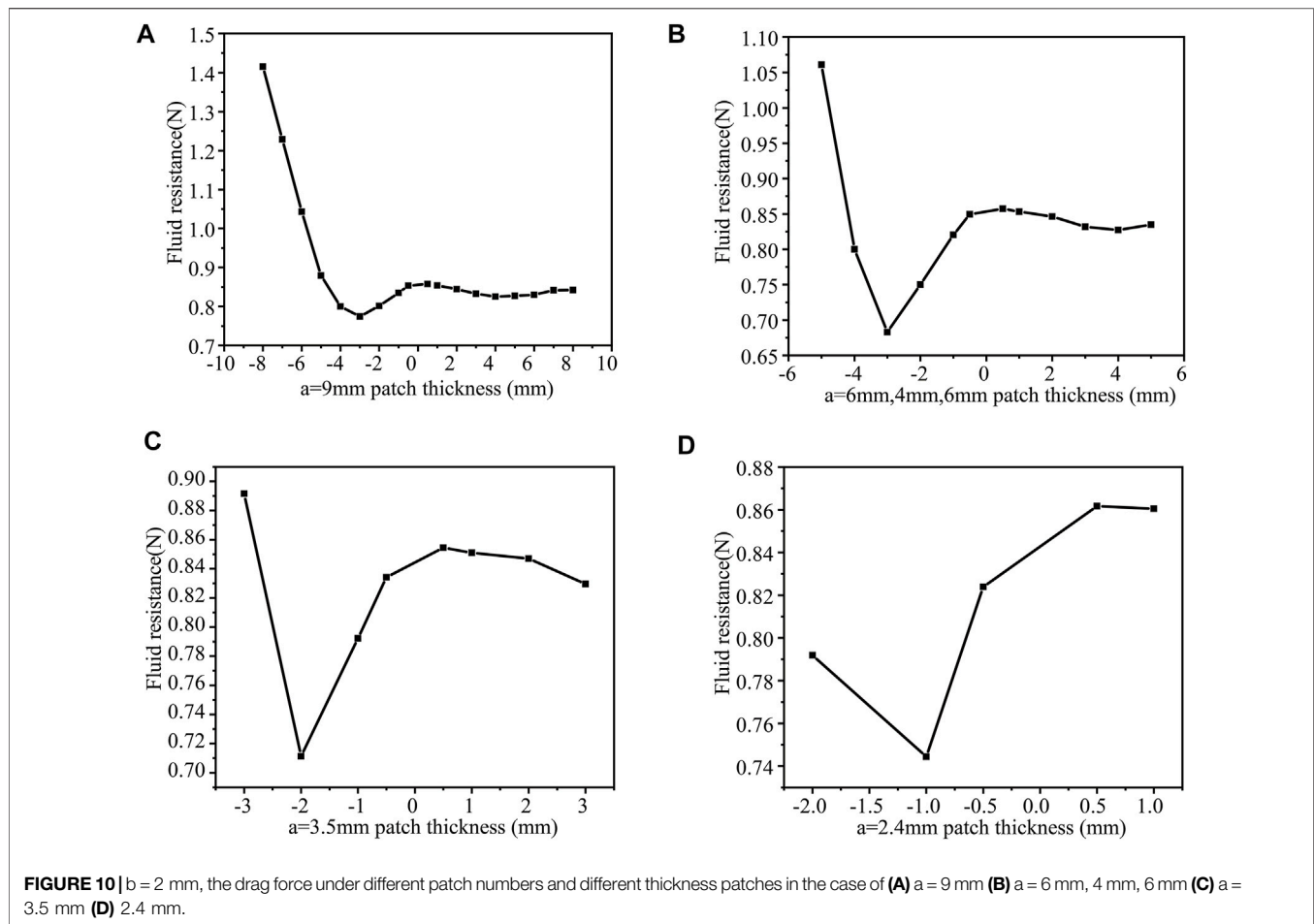
pit ratio are shown in Table 3, and other ratios can be interpolated.

Deep Neural Network Model

The deep neural network (DNN) algorithm was used to build a type prediction model. We use the numerical simulation data to construct a DNN network and randomly divide it into a training and a validation set to construct the prediction model. DNN, also known as a multi-layer perceptual network, is mainly divided into input layer, hidden layer, and output layer. In this study, the conditional data and result data of numerical simulation under multiple sets of working conditions are put into the set network model for training. DNN thoroughly learns the impedance results under different working conditions and assigns the weights of parameters according to the data structure. In this way, DNN can help us predict the resistance effect based on the previously trained model under new working conditions. To guarantee the accuracy of the DNN prediction model, we performed 500 training sessions on the model to find the best parameter combination.

RESULTS

(1) When $b = 10$ mm, $a = 5$ mm, and $n = 1$. The schematic diagram of the model is shown in Figures 6A,B. The results



show that the drag force is the smallest when the patch thickness $h = -1$ mm (0.66477 N). The surface protrusions account for 50% of the entire area, reducing the drag by 22.1%. Then we changed h to calculate the drag force separately ($b = 6$ mm, $n = 1, 2, 3$), as shown in **Figure 7**. When the thickness is $h = -3$ mm ($b = 6$ mm, $a = 7$ mm, $n = 1$), the drag force is the smallest, namely 0.74369 N. The surface protrusion accounts for 30% of the entire area, reducing the drag by 12.9%.

When $b = 6$ mm, $a = 3$ mm, 2 mm, 3 mm, $n = 2$, $h = -2$ mm, the drag force is the least, namely 0.70819 N. Also, the surface protrusion occupies the entire area with 60%, reducing the drag by 17.1%. When $b = 6$ mm, $a = 0.5$ mm, $n = 3$, $h = -0.1$ mm the drag force is the smallest, namely 0.70287 N. The surface protrusion accounts for the entire area 90%, reducing the drag by 17.7%.

When $a = 7$ mm, $h = -5$ mm, the convex structure increased drag force. **Figures 8A–C** shows that not all concave patch structures have increased drag force, and only some are ineffective in reducing drag force. When the surface protrusions account for 90% of the entire area ($n = 3$), the square cylinder has the smallest drag force, 0.70287 N (drag reduction of 17.7%).

(2) When $b = 4$ mm, $n = 1, 2, 3$, then change h to calculate the drag force separately for $a = 8$ mm (**Figure 9A**), $a = 4$ mm (**Figure 9B**), $a = 2$ mm (**Figure 9C**). When the thickness $h = -2$ mm ($b = 4$ mm, $a = 8$ mm, $n = 1$), the drag force is the least, 0.72654 N. The surface protrusions account for 20% of the entire area, reducing the drag by 14.9%. In this case, when the patch size is relatively large, the drag force increase is significant. Consequently, reasonable patch size is essential.

When the patch thickness $h = -0.5$ mm ($b = 4$ mm, $a = 4$ mm, $n = 2$), the drag force is 0.70498 N. The percentage of the surface protrusion to the entire area is 40%, reducing the drag by 17.4%. The concave patch structure also shows increased drag force. The drag force is the smallest (0.69471 N) when $h = -1$ mm ($b = 4$ mm, $a = 2$ mm, $n = 3$). The surface protrusion accounts for 60% of the entire area, reducing the drag by 18.6%.

Taken together, when the surface protrusions account for 40% of the entire area ($n = 2$), the square cylinder has the least drag force, 0.69471 N, reducing the drag by 18.6%.

(3) When $b = 2$ mm, $n = 1, 2, 3, 4$, then change h and calculate the drag force separately $a = 9$ mm (**Figure 10A**), $a = 6$ mm (**Figure 10B**), $a = 3.5$ mm (**Figure 10C**), $a = 2.4$ mm (**Figure 10D**). When the thickness $h = -3$ mm, the drag force is the least, 0.77414 N ($b = 2$ mm, $a = 9$ mm, $n = 1$). The surface

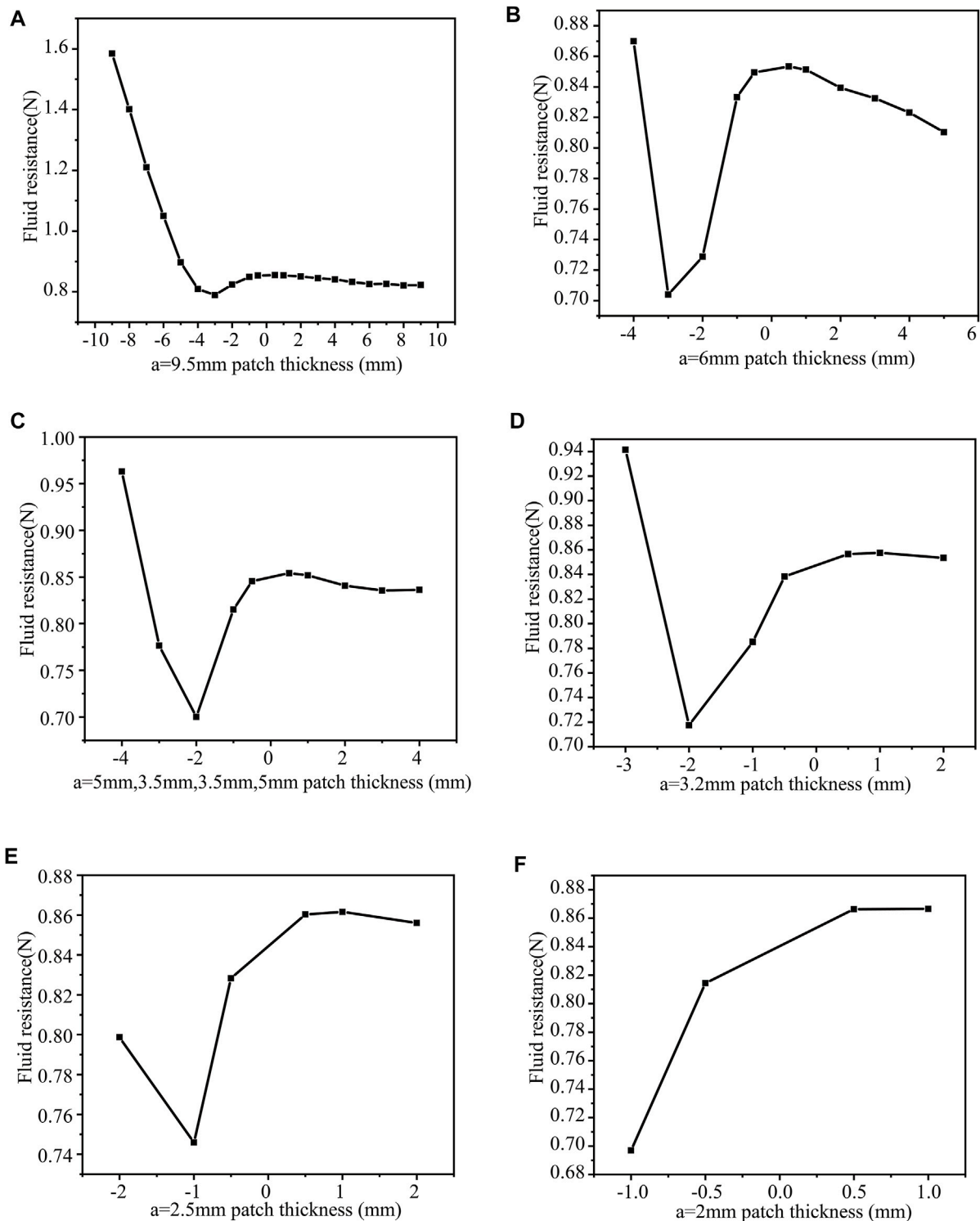


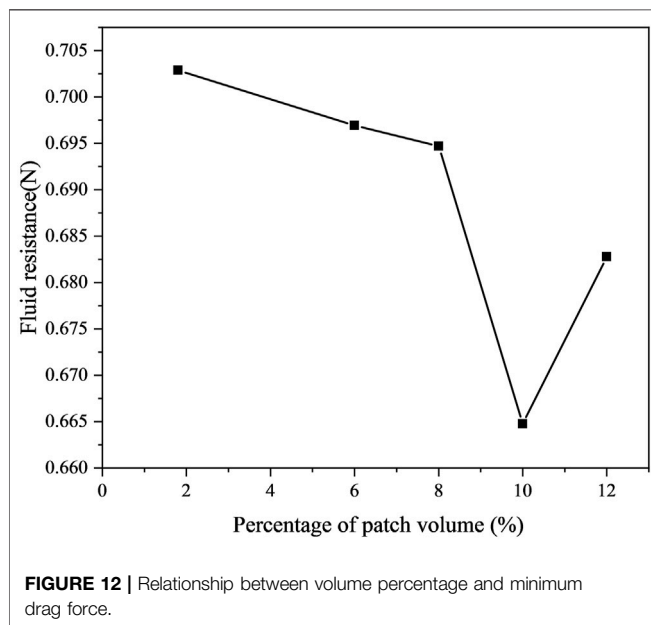
FIGURE 11 | $b = 1$ mm, the number of patches and the drag force under different thickness patches (A) $a = 9.5$ mm; (B) $a = 6$ mm (C) $a = 5$ mm (D) $a = 3.2$ mm (E) $a = 2.5$ mm (F) $a = 2$ mm.

protrusions account for 10% of the entire area, reducing the drag by 9.3%. The situation is the same as before. As a result, drag force is significantly increased when the protrusion size is relatively

large. The drag force is the smallest (0.68278N) when $h = -3$ mm, and the drag force ($b = 2$ mm, $a = 6$ mm, 4 mm, 6 mm, $n = 2$). The surface protrusion occupies 20% of the entire area,

TABLE 4 | The optimal drag reduction structure for each working condition.

No.	Patch length	Number of patches	Patch thickness (convex)	Volume percentage (%)	Minimum drag force (N)
1	1	6	1	6	0.69693
2	2	2	3	12	0.68278
3	4	2	1	8	0.69471
4	6	3	0.1	1.8	0.70287
5	10	1	1	10	0.66477



reducing the drag by 20%. The drag force is the smallest (0.71127N) when the patch thickness $h = -2$ mm ($b = 2$ mm, $a = 3.5$ mm, $n = 3$). The surface protrusion accounts for 30% of the entire area, reducing the drag by 16.7%. The drag force is the smallest 0.74444N when $h = -1$ mm ($b = 2$ mm, $a = 2.4$ mm, $n = 4$). The surface protrusion accounts for 40% of the entire area, reducing the drag by 12.8%.

When the surface protrusion accounts for 20% of the entire area ($n = 2$), the square cylinder has the smallest drag force, 0.68278N, reducing the drag by 20%.

(5) When $b = 1$ mm, $n = 1, 2, 3, 4, 5, 6$, change h and calculate the drag force separately $a = 9.5$ mm (**Figure 11A**), $a = 6$ mm (**Figure 11B**), $a = 3.5$ mm (**Figure 11C**), $a = 2.4$ mm (**Figure 11D**), $a = 2.5$ mm (**Figure 11E**), $a = 2$ mm (**Figure 11F**). When $h = -3$ mm, the drag force is the least, 0.78932N ($b = 1$ mm, $a = 9.5$ mm, $n = 1$). The surface protrusions account for 5% of the entire area, reducing the drag by 7.6%. The drag force is the smallest (0.70387N) when the patch thickness is $h = -3$ mm ($b = 1$ mm, $a = 6$ mm, $n = 2$). The surface protrusion accounts for 10% of the entire area, reducing the drag by 17.6%. The drag force is the smallest 0.70015N when the patch thickness $h = -2$ mm ($b = 1$ mm, $a = 5$ mm, 3.5 mm, 5 mm, $n = 3$). Therefore, surface protrusion accounts for 15% of the entire area, reducing the drag by 18%.

The drag force is the smallest 0.71761N when the patch thickness is $h = -2$ mm ($b = 1$ mm, $a = 3.2$ mm, $n = 4$). Surface protrusion accounts for 20% of the entire area, reducing the drag by 15.9%. The drag force is the smallest 0.74585N when the patch thickness $h = -1$ mm ($b = 1$ mm, $a = 2.5$ mm, $n = 5$). Surface protrusion accounts for 25% of the entire area, reducing the drag by 12.6%. The drag force is the smallest (0.69693N) when the thickness of the patch is $h = -1$ mm ($b = 1$ mm, $a = 2$ mm, $n = 6$). The surface protrusion accounts for 30% of the entire area, reducing the drag by 18.4%.

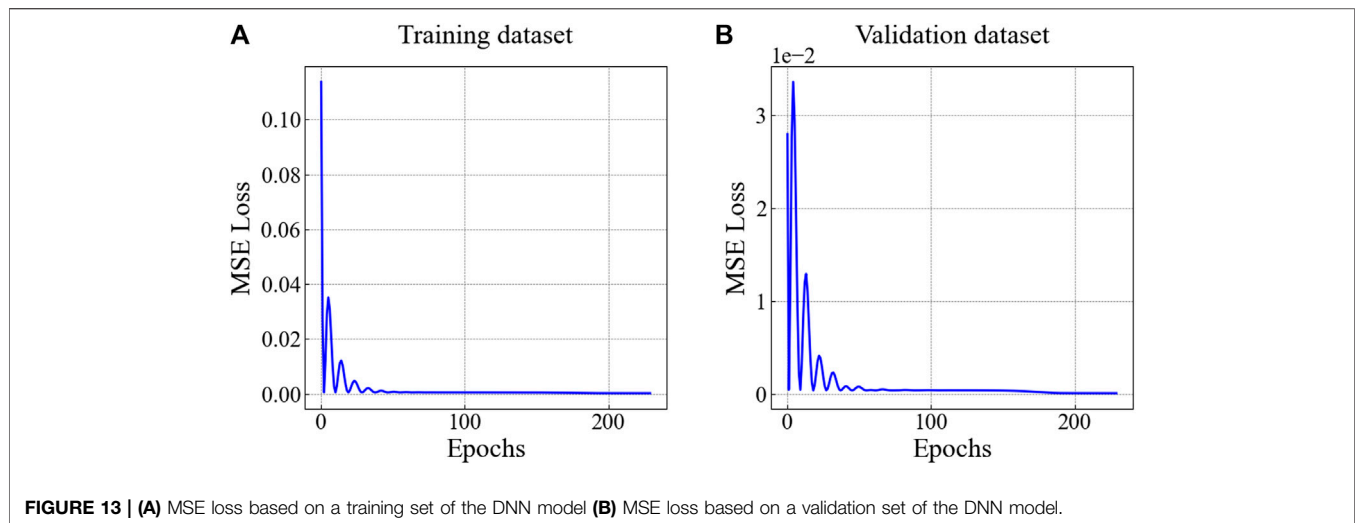
On the whole, when the surface protrusion accounts for 30% of the entire area ($n = 6$), the square cylinder has the least drag force, 0.69693N. At this time, reducing the drag by 18.4%.

Select the optimal drag reduction structure for each working condition, as shown in **Table 4**. The volume percentage and the minimum drag force was shown in **Figure 12**. At the same time, we performed 500 training sessions on the model to find the optimal parameter combination to ensure the accuracy of the DNN prediction model. **Figure 13A** shows the DNN model's training effect based on the drag force data of the numerical simulation. The results indicate that the DNN model based on numerical simulation data has an excellent prediction for drag reduction. Moreover, **Figure 13B** demonstrates the robust performance of trained mature DNN models using the validation dataset. We found that the DNN prediction model has performance, as confirmed by the validation dataset, demonstrating the robustness of the numerical simulation data.

DISCUSSION

Numerical simulation shows that the drag reduction performance of the convex square cylinder is better than that of the concave ones. However, not all raised structures reduced the drag. The drag reduction performance mainly depends on the degree of its protrusion. Too large a protrusion will increase the drag force. However, the drag reduction effect of the concave patch structure is not apparent, and the drag is increased in many cases.

When the fluid particles flow through the front edge of the square cylinder, the surface of the square cylinder will hinder the fluid, and the high-pressure fluid near the front edge promotes the developing boundary layer to gradually develop to both sides of the square cylinder. Blockage occurs under the influence of viscosity, which loses kinetic energy and causes the fluid particles to slow down gradually. At the same time, under the condition of a high Reynolds number, the force generated by the pressure is



not enough to surround the entire back of the square cylinder. Still, a separation point is generated near the maximum width of the square cylinder section, and the separated fluid forms an unstable shear layer. Since the flow velocity of the outer part near the free flow area is greater than that of the inner part, the fluid tends to rotate and disperse into several vortices. In addition, during the downstream movement of the vortex, the strength of the vortex gradually weakens due to the existence of fluid viscosity. After the boundary layer detaches from the surface of the square cylinder at the separation point, a wake area is formed at the tail of the square cylinder, and the surrounding flow resistance is formed under the action of the pressure difference between the front edge of the square cylinder and the wake area. When the separation point is further back, the wake area is smaller, and the pressure difference resistance acting on the square cylinder is smaller to reduce resistance.

The protrusion patch has a noticeable drag reduction, whereas the pit patch increases the drag. Similar results have been reported in other kinds of literature. Ueda et al. (2009) used numerical and experimental methods to visualize the flow around a square cylinder with a chamfered front edge to explore its drag reduction mechanism. Although the square-pillar structure of the literature is different from that of this study, they are all convex structures, which also achieve a better drag reduction effect. Kurata et al. (2009) studied the drag reduction of a right-angled cylinder with a leading-edge chamfer and an aspect ratio of less than or equal to the unit, which is also a convex structure and has a better drag reduction effect. However, they only explored the drag reduction of a convex side without considering the pits. The study further changed the structure of the four directions of the square cylinder. Thus, the work made a supplement to the research of others. The structure of the square cylinder in this article also has a better drag reduction performance.

Song et al. (2019) studied the drag reduction of the grooved cylinder, and the results showed that under the supercritical Reynolds number, the drag reduction is significant under the

appropriate groove structure parameters. The results show that the drag force reduction of the pit-patched square cylinder is not significant. The limited selection of pit sizes may increase the drag force. This is also a supplement to the work of others.

We use the passive control method to study square cylinder drag reduction, which is similar to Jin et al. For drag reduction, the passive control method is usually used to cut corners at the front edge of a square cylinder. First, Jin adopts the previously studied control method (called CM-1, or control method 1) and conducts numerical research. On this basis, a new control method was proposed. That is, an additional cut corner (CM-2, control method 2) was used to test the performance of the drag reduction. Both control methods of CM-1 and CM-2 provide significant drag reduction. The drag reduction is as high as 48% and 61%, respectively, compared with the smooth square cylinder. In addition, the newly proposed control method is more effective than the previous control method (Jin et al., 2019).

Numerous researchers have previously investigated the drag reduction of hollow cylinders. Durhasan (2020) studied the drag reduction of hollow cylinders with slits. He observed all the gap ratio structures compared with solid cylinders. The slit cylinders have reduced the drag coefficient by 42%. Wei et al. (2013) used computational fluid dynamics (CFD) methods to analyze the drag reduction ability of triangular grooves on the flow in the pipe. The study found that the triangular groove structure weakened the velocity fluctuation and intensity of the turbulent burst of the boundary layer and macroscopically reduced the velocity gradient in the near-wall area, thereby reducing the surface frictional drag force, with a maximum drag reduction rate of 6.93%. We applied the same numerical simulation method. The cylindrical pipe they studied and our square cylinder can be used as an analogy reference. Yanuar et al. (2017) studied the influence of agar jelly coating on the flow drag force reduction in rectangular pipes, and the results showed that the maximum drag force reduction was about 19%. They also use a passive control method to study the drag reduction mechanism through additive polymers.

The splitter plate may achieve a good performance of drag reduction of the square cylinders. Dash et al. (2020) carried out a numerical study on the drag force reduction of the square cylinder using the double splitter plate. The study showed that the double splitter plate suppressed the shedding of the von Karman vortex and lift fluctuations and produced good drag reduction ($\approx 21\%$) when less than half the length of the single splitter plate. However, Ma et al. (2018) applied comprehensive methods to promote drag reduction performance further. They numerically simulate the drag reduction in a structure with round rods arranged upstream of the square cylinder and a splitter plate downstream. The study shows that the average drag coefficient of the maximum percentage reduction is 68.76%. Although the passive control methods adopted by these researchers are different, they have achieved different levels of drag reduction. Data fusion technology and intelligent algorithms may help flow forecasting (Sun et al., 2020b; Sun et al., 2020c; Tan et al., 2020). The DNN method in this study also showed excellent prediction performance.

CONCLUSION

Under the typical high Reynolds number $Re = 40,000$, this study uses the Spalart-Allmaras turbulence model to calculate the flow field. Based on verifying the accuracy of the numerical results, the effect of different patch sizes on the drag force of the square cylinder is studied. The convex square cylinder of the patch has a better drag reduction effect than the concave patch. Concave patches do not significantly reduce drag and sometimes even

REFERENCES

- Bahrami, A., and Hacısevki, H. (2019). Comparison of Flow Structures in the Wake Region of a Square Cylinder or a U Shape Cylinder. *Ocean. Eng.* 187, 106211. doi:10.1016/j.oceaneng.2019.106211
- Bearman, P. W. (1998). Developments in the Understanding of Bluff Body Flows. *JSM E Int. J. Ser. B, Fluids Therm. Eng.* 41, 103–114. doi:10.1299/jsmeb.41.103
- Behera, S., and Saha, A. K. (2021). Effect of Inlet Shear on Turbulent Flow Past a Wall-Mounted Finite-Size Square Cylinder. *Ocean. Eng.* 234, 109270. doi:10.1016/j.oceaneng.2021.109270
- Chen, Y. (2019). *Aerodynamics of Smooth and Turbulent Flows Past Stationary and Oscillating Square Cylinders*. Southampton.
- Costantini, R., Mollicone, J.-P., and Battista, F. (2018). Drag Reduction Induced by Superhydrophobic Surfaces in Turbulent Pipe Flow. *Phys. Fluids* 30, 025102. doi:10.1063/1.5011805
- Dash, S. M., Triantafyllou, M. S., and Alvarado, P. V. Y. (2020). A Numerical Study on the Enhanced Drag Reduction and Wake Regime Control of a Square Cylinder Using Dual Splitter Plates. *Comput. Fluids* 199, 104421. doi:10.1016/j.compfluid.2019.104421
- Durhasan, T. (2020). Flow Topology Downstream of the Hollow Square Cylinder with Slots. *Ocean. Eng.* 209, 107518. doi:10.1016/j.oceaneng.2020.107518
- He, G. S., Li, N., and Wang, J. J. (2014). Drag Reduction of Square Cylinders with Cut-Corners at the Front Edges. *Exp. FLUIDS* 55, 1–11. doi:10.1007/S00348-014-1745-1
- Huang, L., Chen, C., Yun, J., Sun, Y., Tian, J., Hao, Z., et al. (2022). Multi-scale Feature Fusion Convolutional Neural Network for Indoor Small Target Detection. *Front. Neurobotics* 16, 881021. doi:10.3389/fnbot.2022.881021
- Huang, L., Fu, Q., He, M., Jiang, D., and Hao, Z. (2021). Detection Algorithm of Safety Helmet Wearing Based on Deep Learning. *Concurr. Comput. Pract. Exper* 33, 1–14. doi:10.1002/cpe.6234
- Igarashi, T. (1997). Drag Reduction of a Square Prism by Flow Control Using a Small Rod. *J. Wind Eng. Industrial Aerodynamics* 69–71, 141–153. doi:10.1016/S0167-6105(97)00150-5
- Jiang, D., Li, G., Sun, Y., Hu, J., Yun, J., and Liu, Y. (2021a). Manipulator Grabbing Position Detection with Information Fusion of Color Image and Depth Image Using Deep Learning. *J. Ambient. Intell. Hum. Comput.* 12, 10809–10822. doi:10.1007/s12652-020-02843-w
- Jiang, D., Li, G., Tan, C., Huang, L., Sun, Y., and Kong, J. (2021b). Semantic Segmentation for Multiscale Target Based on Object Recognition Using the Improved Faster-RCNN Model. *Future Gener. Comput. Syst.* 123, 94–104. doi:10.1016/j.future.2021.04.019
- Jin, Y., Cheng, Z., Han, X., Mao, J., and Jin, F. (2019). VLES of Drag Reduction for High Reynolds Number Flow Past a Square Cylinder Based on OpenFOAM. *Ocean. Eng.* 190, 106450. doi:10.1016/j.oceaneng.2019.106450
- Kim, D.-J., and Kim, K.-J. (2012). Control of Square Cylinder Flow Using Plasma Synthetic Jets. *J. Comput. fluids Eng.* 17, 85–92. doi:10.6112/KSCFE.2012.17.2.085
- Koide, M., Okanaga, H., and Aoki, K. (2006). Drag Reduction Effect of Square Cylinders by Grooves and Corner-Cuttings. *J. Vis. Soc. Jpn.* 26, 69–72. doi:10.3154/jvs.26.supplement1_69
- Kurata, M., Ueda, Y., Kida, T., and Iguchi, M. (2009). Drag Reduction Due to Cut-Corners at the Front-Edge of a Rectangular Cylinder with the Length-To-Breadth Ratio Being Less Than or Equal to Unity. *J. Fluids Eng.* 131, 1–5. doi:10.1115/1.3129123
- Lahaye, A., Leroy, A., and Kourta, A. (2014). Aerodynamic Characterisation of a Square Back Bluff Body Flow. *Ijad* 4, 43–60. doi:10.1504/ijad.2014.057804
- Lesage, F., and Gartshore, I. S. (1987). A Method of Reducing Drag and Fluctuating Side Force on Bluff Bodies. *J. Wind Eng. Industrial Aerodynamics* 25, 229–245. doi:10.1016/0167-6105(87)90019-5

DATA AVAILABILITY STATEMENT

The raw data supporting the conclusion of this article will be made available by the authors, without undue reservation.

AUTHOR CONTRIBUTIONS

Conceptualization, SW; data curation, QW; writing—original draft preparation, SW and QW; writing—review and editing, SW and XS; supervision and project administration, SW and XS. All authors have read and agreed to the published version of the manuscript.

FUNDING

This research was supported by the CRSRI Open Research Program (Program SN: CKWV2018459/KY) and the National Natural Science Foundation of China (51922065).

- Lorite-Diez, M., Jiménez-González, J. I., Pastur, L., Cadot, O., and Martínez-Bazán, C. (2020). Drag Reduction on a Three-Dimensional Blunt Body with Different Rear Cavities under Cross-Wind Conditions. *J. Wind Eng. Industrial Aerodynamics* 200, 104145. doi:10.1016/j.jweia.2020.104145
- Luo, B., Sun, Y., Li, G., Chen, D., and Ju, Z. (2020). Decomposition Algorithm for Depth Image of Human Health Posture Based on Brain Health. *Neural Comput. Applic* 32, 6327–6342. doi:10.1007/s00521-019-04141-9
- Ma, R., Zhang, L., Li, G., Jiang, D., Xu, S., and Chen, D. (2020). Grasping Force Prediction Based on sEMG Signals. *Alexandria Eng. J.* 59, 1135–1147. doi:10.1016/j.aej.2020.01.007
- Ma, Y., Rashidi, M. M., and Yang, Z.-g. (2018). Numerical Simulation of Flow Past a Square Cylinder with a Circular Bar Upstream and a Splitter Plate Downstream. *J. Hydrodyn.* 31, 949–964. doi:10.1007/S42241-018-0087-5
- Mangal, M., Agarwal, P. K., and Behl (2014). *Drag Reduction of a Square Cylinder with Upstream Rod Arrangement and its Computational Analysis*. Ghaziabad: National Conference on Recent Advances In Mechanical & Civil Engineering.
- Shui, Q., Duan, C., Wang, D., and Gu, Z. (2021). New Insights into Numerical Simulations of Flow Around Two Tandem Square Cylinders. *AIP Adv.* 11, 045315. doi:10.1063/5.0042797
- Song, X., Qi, Y., Zhang, M., Zhang, G., and Zhan, W. (2019). Application and Optimization of Drag Reduction Characteristics on the Flow Around a Partial Grooved Cylinder by Using the Response Surface Method. *Eng. Appl. Comput. Fluid Mech.* 13, 158–176. doi:10.1080/19942060.2018.1562382
- Sun, Y., Hu, J., Li, G., Jiang, G., Xiong, H., Tao, B., et al. (2020a). Gear Reducer Optimal Design Based on Computer Multimedia Simulation. *J. SUPERCOMPUT* 76, 4132–4148. doi:10.1007/s11227-018-2255-3
- Sun, Y., Tian, J., Jiang, D., Tao, B., Liu, Y., Yun, J., et al. (2020b). Numerical Simulation of Thermal Insulation and Longevity Performance in New Lightweight Ladle. *Concurr. Comput. Pract. Exper* 32, 1532–1546. doi:10.1002/cpe.5830
- Sun, Y., Xu, C., Li, G., Xu, W., Kong, J., Jiang, D., et al. (2020c). Intelligent Human Computer Interaction Based on Non Redundant EMG Signal. *Alexandria Eng. J.* 59, 1149–1157. doi:10.1016/j.aej.2020.01.015
- Tan, C., Sun, Y., Li, G., Jiang, G., Chen, D., and Liu, H. (2020). Research on Gesture Recognition of Smart Data Fusion Features in the IoT. *Neural Comput. Applic* 32, 16917–16929. doi:10.1007/s00521-019-04023-0
- Tong, J. C. K., Abraham, J. P., Tse, J. M. Y., and Sparrow, E. M. (2015). Using Corner Chamfers to Reduce the Drag of Flat-Sided Columns. *Proc. Institution Civ. Eng. - Eng. Comput. Mech.* 168, 79–88. doi:10.1680/EACM.14.00023
- Ueda, Y., Kurata, M., Kida, T., and Iguchi, M. (2009). Visualization of Flow Past a Square Prism with Cut-Corners at the Front-Edge. *J. Vis.* 12, 383–391. doi:10.1007/BF03181881
- Vikram, C. K., Ravindra, H. V., and Krishnegowda, Y. T. (2020). Visualization of Flow Past Square Cylinders with Corner Modification. *J. Mech. Energy Eng.* 4, 285–294. doi:10.30464/jmee.2020.4.3.285
- Wang, Q., Jiang, Q., Hu, G., Chen, X., Li, C., and Xiao, Y. (2021). Aerodynamic Characteristics of a Square Cylinder with Corner Fins. *Aben* 2, 1–20. doi:10.1186/S43251-021-00042-X
- Wei, Z. G., Li, Y., Ke, Z. W., and Li, X. L. (2013). Numerical Simulation of Internal Flow Drag Reduction with Triangular Riblet Surface. *Amr* 779-780, 401–405. doi:10.4028/www.scientific.net/amr.779-780.401
- Yang, F., Zhou, Z., Tang, G., and Lu, L. (2021). Steady Flow Around a Square Cylinder Near a Plane Boundary. *Ocean. Eng.* 222, 108599. doi:10.1016/J.OCEANENG.2021.108599
- Yanuar, G., Gunawan, K. T., Waskito, K. T., and Ogata, S. (2017). Effect of Agar Jelly Coating in Rectangular Pipe to Flow Drag Reduction. *Jafm* 10, 1161–1166. doi:10.18869/acadpub.jafm.73.241.26701
- Yen, S. C., and Wu, S. F. (2012). Square-Cylinder Flow Characteristics Modulated Using Upstream Control Rod. *J. Mech.* 28, 279–289. doi:10.1017/jmech.2012.31
- Zhao, C., Wang, H., Zhaom, X., and Zhao, X. (2021). Effects of Oncoming Flow Turbulence on the Near Wake and Forces of a 3D Square Cylinder. *J. Wind Eng. Industrial Aerodynamics* 214, 104674. doi:10.1016/J.jweia.2021.104674

Conflict of Interest: The authors declare that the research was conducted in the absence of any commercial or financial relationships that could be construed as a potential conflict of interest.

Publisher's Note: All claims expressed in this article are solely those of the authors and do not necessarily represent those of their affiliated organizations, or those of the publisher, the editors, and the reviewers. Any product that may be evaluated in this article, or claim that may be made by its manufacturer, is not guaranteed or endorsed by the publisher.

Copyright © 2022 Wang, Wu and Shi. This is an open-access article distributed under the terms of the Creative Commons Attribution License (CC BY). The use, distribution or reproduction in other forums is permitted, provided the original author(s) and the copyright owner(s) are credited and that the original publication in this journal is cited, in accordance with accepted academic practice. No use, distribution or reproduction is permitted which does not comply with these terms.